Jagannath University Journal of Science
Volume 10, Number II, Dec. 2023, pp. 75−86
https://jnu.ac.bd/journal/portal/archives/science.jsp
ISSN 3005-4486 (Online), ISSN 2224-1698 (Print)

Heat Transfer Characteristics of Al_2O_3-Cu/Water Hybrid Nanofluid inside a Square Cavity in the Presence of Inclined Periodic Magnetic Field

Research Article

Md. Nurul Huda[1,*], Md. Shariful Alam[1] and S. M. Chapal Hossain[2]

[1]*Department of Mathematics, Jagannath University, Dhaka-1100, Bangladesh*
[2]*Department of Applied Mathematics, University of Dhaka, Dhaka-1000, Bangladesh*

DOI: https://doi.org/10.3329/jnujsci.v10i2.71257

Received: 7 August 2023, Accepted: 13 September 2023

ABSTRACT

The goal is to scrutinize the thermal features of hybrid nanofluid in a square cavity with the effect of oblique periodic magnetic field. The modified hybrid nanofluid is a combination of nanoparticles Al_2O_3, Cu and base fluid water with equal volume fraction of Al_2O_3 and Cu.

The finite element method based Galerkin weighted residual scheme is chosen to find the solution of the non-dimensional governing equations. The effects of different model factors such as oblique angle and period of the periodic magnetic field, Hartmann number, Rayleigh number, nanoparticles volume fraction on the heat transfer are scrutinized. The outcomes are exhibited with the help of isotherms and average Nusselt number as well. The numerical results show that when the period of the slanted periodic magnetic field increases gradually, the distinct model factors (Rayleigh number, nanoparticles volume fraction, and slanting angle) raise the heat transfer rate progressively, whereas augmentation of the Hartmann number diminutions the entire heat transfer rate.

Keywords: *Hybrid nanofluid, Brownian motion, Oblique periodic magnetic field, Finite element method*

1. Introduction

Enhancement of heat transfer (HT) rate in thermal systems has been one of the major expectations of scientists. Numerous dissimilar methods were applied to progress the HT rate for arriving a suitable position of thermal efficiency (TE) while enriching in the thermal conductivity (TC). Moreover, nanofluid (NF) with the composed of nanoparticles (NPs) and base fluid (BF) has been introduced as a higher workable HT medium in sight of its relatively higher TC. At first (Maxwell 1873, Choi 1995) display the opportunity of rise of TC of a solid-liquid mixing by growing the volume fraction (VF) of NPs. From then onwards, comprehensive examinations have been guided either analytically (Ho et al. 20l0, Saghir and Rahman 2020) or numerically (Oztop and Abu Nada 2008, Alam et al. 2016) to examine the original features of nanofluids (NFs). This study settled that NFs may display advanced TC other than the BF. Recently, an empirical study was performed on NF with distinct sorts of NPs spread in a BF which is called a hybrid nanofluid (H-NF) (Suresh et al. 2011). H-NF is a new type of NF

***Corresponding author:** Md. Nurul Huda
E-mail: mnurulhdu1@gmail.com

(next generation NFs), that process several possible applications in usual fields of HT. This H-NF may have TC larger than that of the simple NF (Jana et al. 2007).

Additionally, many inquiries have been completed with distinct sorts of hybrid nanofluids (H-NFs) in assorted domains (Esfe et al. 2016, Devi and Devi. 20l7, Belhaj and Ben-Beya 2022). The finding is that the HT rate may be upper for the H-NF other than the simple NF and the HT rate differs from model to model, NF to NF with usage of the thermophysical correlations (TPCs) of NFs. It is to be mentioned here that no such single TPCs are settled for the thermophysical properties (TP) of H-NFs.

For real life uses, (Selvakumar and Suresh 2012) applied $Cu-Al_2O_3/water$ H-NF and measured TE in the electrical heat sink. They found 12.61% augmented pumping power and 24.35% heat improvement, applying 0.1% VF of H-NF compared to pure water for a uniformly heated circular tube with fixed volumetric flow rate. (Nasrin et al. 2020) conducted a numerical analysis dealing with the natural convection of H-NFs $(Cu-Al_2O_3/water, Cu-CuO/water$ and $Cu-CNT/water)$ in a lid driven sinusoidal trapezoidal cavity. They exhibited that using H-NF may be helpful to obtained awaited TE and HT rate may rise 15% by growing the Richardson number from 0.1 to 10. (Tayebi and Oztop, 2020) leaded a mathematical study applying $Al_2O_3-Cu/water$ H-NF that yielded the entropy approach for the convective flow between two confocal elliptic cylinders and found the convective flow and thermal features in a H-NF comparative to pure water. (Izadi et al. 2020) deliberate the natural convective HT of H-NF $Ag-MgO/water$ with the impact of slanted periodic magnetic field (PMF) in a four-sided cavity containing a porous case modeled by Brinkman-extended Darcy model. Their results show that for HT and fluid flow, the angle of the IPMF is a good controller parameter. Recently, (Rahman et al. 2022) inspected the natural convective HT efficiency in $Al_2O_3-Cu/water$ H-NF with recto-trapezoidal cavity. Their results presented that thermal buoyancy parameter strongly controls the patterns of isotherms, heat lines and streamlines. They also calculate the HT coefficient, TE index and friction factor and for lower Rayleigh number *(Ra)* they obtained the higher TE.

For the aforesaid frequent benefits of H-NF based solar thermal collectors, diverse geometrical shapes of solar thermal collectors have been considered in former reports for unlike available NFs with dissimilar TPCs. Although momentous research is completed on the $Al_2O_3-Cu/water$ H-NF, still there is a room for further examination using proper TPCs to build an advanced mathematical model. Therefore, the object is to study the time-variant free convective HT of $Al_2O_3-Cu/water$ H-NF in a quadrate cavity with the effect of oblique PMF. The numerical results could be beneficial for design optimization as well as for TP improvement of thermal schemes such as solar thermal collectors and cooling of electronic equipment.

2. Methodologies

2.1. Physical model

In this problem, an IPMF is attributed on a time-variant, laminar, incompressible, 2D convective flow of H-NF in a four-sided cavity of length *L* as Figure 1. The cavity walls are measured as fixed and convection initiated with making temperature differences between cold and heated walls. The oblique PMF depends on the *x*- and *y*-coordinate systems and this relation is stated as $B=B_0\sin[\frac{2\pi}{\lambda_0}(x\cos\gamma+y\sin\gamma)]$, where λ_0, the period, and B_0, amplitude, and γ, the leaning angle with the route of the applied PMF to the horizontal positive *x*-axis. The left wall of the cavity is uniformly heated at temperature $(T=T_h)$, the right wall is cooled at lower temperature $(T=T_{c_1})$ and other two walls are insulated. Noted that thermal steadiness occurs in the BF and NPs as well. In the flow domain chemical reactions and thermal radiations are neglected. The properties of the H-NF are assumed to be constant excluding the density variant in the body force which is evaluated by the Boussinesq estimation. The gravity deeds in the negative *y*-direction, and the Brownian motion (BM) of the NPs are included in the TC model. All walls are taken to be rigid and no-slip approach. Table 1 shows the thermal properties used in this study.

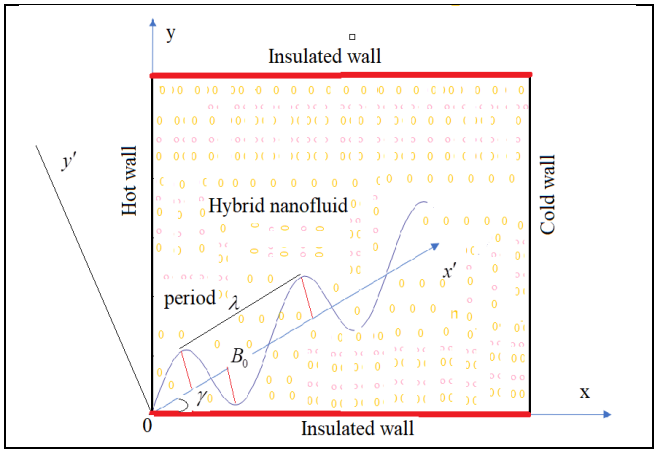

Fig. l: Schematic view of the square cavity with thermal settings.

Table l: Thermal properties used in this study (Oztop and Abu-Nada 2008).

BF and NPs	c_p (J/kgK)	ρ (kg/m^3)	κ (W/mK)	$\beta\times10^{-5}$ $(1/K)$	μ (Ns/m^2)	σ (S/m)	Pr
Water	4179	997.1	0.613	21	0.001003	5.5×10^{-6}	6.8377
Cu	385	8933	400	1.67		59.6×10^{6}	
Al_2O_3	765	3970	40	0.85		35×10^{6}	

2.2. Mathematical model

Based on the aforementioned postulates, the time-variant 2D H-NF flow describe by the following model equations comprising continuity, momentum, and energy equations (Belhaj and Ben-Beya 2022):

$$\frac{\partial u}{\partial x}+\frac{\partial v}{\partial y}=0 \tag{1}$$

$$\frac{\partial u}{\partial t}+u\frac{\partial u}{\partial x}+v\frac{\partial u}{\partial y}=-\frac{1}{\rho_{hnf}}\frac{\partial p}{\partial x}+\frac{\mu_{hnf}}{\rho_{hnf}}\left(\frac{\partial^2 u}{\partial x^2}+\frac{\partial^2 u}{\partial y^2}\right)$$
$$+\frac{\sigma_{hnf}B_0^2}{\rho_{hnf}}\sin^2[\tfrac{2\pi}{\lambda_0}\left(x\cos\gamma+y\sin\gamma\right)](v\sin\gamma\cos\gamma-u\sin^2\gamma\Big) \tag{2}$$

$$\frac{\partial v}{\partial t}+u\frac{\partial v}{\partial x}+v\frac{\partial v}{\partial y}=-\frac{1}{\rho_{hnf}}\frac{\partial p}{\partial y}+\frac{\mu_{hnf}}{\rho_{hnf}}\left(\frac{\partial^2 v}{\partial x^2}+\frac{\partial^2 v}{\partial y^2}\right)+g\left(T-T_C\right)\frac{(\rho\beta)_{hnf}}{\rho_{hnf}}$$
$$+\frac{\sigma_{hnf}B_0^2}{\rho_{hnf}}\sin^2[\tfrac{2\pi}{\lambda_0}(x\cos\gamma+y\sin\gamma)]\left(u\sin\gamma\cos\gamma-v\cos^2\gamma\right) \tag{3}$$

$$\frac{\partial T}{\partial t}+u\frac{\partial T}{\partial x}+v\frac{\partial T}{\partial y}=\alpha_{hnf}\left(\frac{\partial^2 T}{\partial x^2}+\frac{\partial^2 T}{\partial y^2}\right) \tag{4}$$

where the model variables and quantities are described in the nomenclature.

2.3. Initial and boundary conditions

For $t=0$,

entire domain: $u=0, v=0, T=T_{c_1}, p=0$ (5a)

For $t>0$,

At the left hot wall: $u=0, v=0, T=T_h$ (5b)

At the top and bottom insulated walls:

$$u = 0, v = 0, \frac{\partial T}{\partial y} = 0 \tag{5c}$$

At the right cold wall: $u = 0, v = 0, T = T_{c_1}$ (5d)

2.4. Thermo-physical properties

For the present H-NF problem, NPs VF of H-NF, viscosity, density, thermal diffusivity, heat capacitance, electrical conductivity, thermal expansion coefficient and TC of H-NF have been taken into consideration respectively as follows (Rahman et al. 2022):

$$\phi_{hnp} = \phi_{Al_2O_3} + \phi_{Cu} \tag{6}$$

$$\mu_{hnf} = \frac{\mu_{bf}}{\left(1-\phi_{hnp}\right)^{2.5}} \tag{7}$$

$$\rho_{hnf} = \rho_a\phi_{Al_2O_3} + \rho_c\phi_{Cu} + (1-\phi_{hnp})\rho_{bf} \tag{8}$$

$$\alpha_{hnf} = \frac{\kappa_{hnf}}{(\rho C_p)_{hnf}} \tag{9}$$

$$(\rho C_p)_{hnf} = \phi_{Al_2O_3}(\rho C_p)_a + \phi_c(\rho C_p)_c + (1-\phi_{hnp})(\rho C_p)_{bf} \tag{10}$$

$$\sigma_{hnf} = \sigma_{bf} + \frac{3\sigma_{bf}(\sigma_{np}-\sigma_{bf})\phi_{hnp}}{(\sigma_{np}+2\sigma_{bf})-(\sigma_{np}-\sigma_{bf})\phi_{hnp}} \tag{11}$$

$$(\rho\beta)_{hnf} = \phi_{Al_2O_3}(\rho\beta)_a + \phi_{Cu}(\rho\beta)_c + (1-\phi_{hnp})(\rho\beta)_{bf} \tag{12}$$

$$\kappa_{hnf} = \frac{\frac{\phi_{Al_2O_3}\kappa_a+\phi_{Cu}\kappa_c}{\phi_{hnp}} + 2\kappa_{bf} + 2(\phi_{Al_2O_3}\kappa_a+\phi_{Cu}\kappa_c) - 2\phi_{hnp}\kappa_{bf}}{\frac{\phi_{Al_2O_3}\kappa_a+\phi_{Cu}\kappa_c}{\phi_{hnp}} + 2\kappa_{bf} - (\phi_{Al_2O_3}\kappa_a+\phi_{Cu}\kappa_c) + \phi_{hnp}\kappa_{bf}}\kappa_{bf} \text{ (without Brownian effect)} \tag{13a}$$

$$\kappa_{hnf} = \frac{\frac{\phi_{Al_2O_3}\kappa_a+\phi_{Cu}\kappa_c}{\phi_{hnp}} + 2\kappa_{bf} + 2(\phi_{Al_2O_3}\kappa_a+\phi_{Cu}\kappa_c) - 2\phi_{hnp}\kappa_{bf}}{\frac{\phi_{Al_2O_3}\kappa_a+\phi_{Cu}\kappa_c}{\phi_{hnp}} + 2\kappa_{bf} - (\phi_{Al_2O_3}\kappa_a+\phi_{Cu}\kappa_c) + \phi_{hnp}\kappa_{bf}}\kappa_{bf} + \frac{(\rho C_p)_{np}\phi_{hnp}}{2D_T^l}\sqrt{\frac{2k_BD_T T_{ref}}{3\pi d_p\mu_{hnf}}} \tag{13b}$$

where $\sigma_{np} = \dfrac{\phi_{Al_2O_3}\sigma_a + \sigma_c\phi_{Cu}}{\phi_{hnp}}$, $(\rho C_p)_{np} = \dfrac{\phi_{Al_2O_3}(\rho C_p)_a + \phi_{Cu}(\rho C_p)_c}{\phi_{hnp}}$

and $D_T = 0.126\dfrac{\kappa_{hnf}\beta_{bf}\mu_{hnf}(0.0002d_p+0.1537)}{\kappa_{bf}\rho_{hnf}}, D_T^l = \sqrt{D_T}$

and T_{ref} is the reference temperature. All the symbols and the associated factors are demarcated in the nomenclature.

2.5. Non-dimensional formulation

Now using the dimensional equations (1)-(4) and the dimensionless variables in (14), we create the following dimensionless governing equations (15)-(18).

$$\left.\begin{aligned} X = \frac{x}{L}, Y = \frac{y}{L}, U = \frac{uL}{\alpha_{bf}}, V = \frac{vL}{\alpha_{bf}}, P = \frac{pL^2}{\rho_{bf}\alpha_{bf}^2}, \\ \theta = \frac{T-T_{c_1}}{T_h-T_{c_1}}, \tau = \frac{t\alpha_{bf}}{L^2}, \upsilon_{bf} = \frac{\mu_{bf}}{\rho_{bf}}, \lambda = \frac{\lambda_0}{L} \end{aligned}\right\} \tag{14}$$

$$\frac{\partial U}{\partial X} + \frac{\partial V}{\partial Y} = 0 \tag{15}$$

$$A\left(\frac{\partial U}{\partial \tau} + U\frac{\partial U}{\partial X} + V\frac{\partial U}{\partial Y}\right) = -\frac{\partial P}{\partial X} + B\,\mathrm{Pr}\left(\frac{\partial^2 U}{\partial X^2} + \frac{\partial^2 U}{\partial Y^2}\right) + E\,\mathrm{Pr}\,Ha^2\sin^2\left[\tfrac{2\pi}{\lambda}(X\cos\gamma + Y\sin\gamma)\right]\left(V\cos\gamma\sin\gamma - U\sin^2\gamma\right) \tag{16}$$

$$A\left(\frac{\partial V}{\partial \tau} + U\frac{\partial V}{\partial X} + V\frac{\partial V}{\partial Y}\right) = -\frac{\partial P}{\partial Y} + BPr\left(\frac{\partial^2 V}{\partial X^2} + \frac{\partial^2 V}{\partial Y^2}\right) + CRa\,\mathrm{Pr}\,\theta + E\,\mathrm{Pr}\,Ha^2\sin^2\left[\tfrac{2\pi}{\lambda}(X\cos\gamma + Y\sin\gamma)\right]\left(U\cos\gamma\sin\gamma - V\cos^2\gamma\right) \tag{17}$$

$$\frac{\partial\theta}{\partial\tau} + U\frac{\partial\theta}{\partial X} + V\frac{\partial\theta}{\partial Y} = D\left(\frac{\partial^2\theta}{\partial X^2} + \frac{\partial^2\theta}{\partial Y^2}\right) \tag{18}$$

where, $A = \dfrac{\rho_{hnf}}{\rho_{bf}}$, $B = \dfrac{\mu_{hnf}}{\mu_{bf}}$, $C = \dfrac{(\rho\beta)_{hnf}}{(\rho\beta)_{bf}}$,

$D = \dfrac{\kappa_{hnf}}{\kappa_{bf}} / \dfrac{(\rho C_p)_{hnf}}{(\rho C_p)b_{bf}}$, $E = \dfrac{\sigma_{hnf}}{\sigma_{bf}}$,

$Ra = \dfrac{g\beta_{bf}\left(T_h - T_{c_1}\right)L^3}{\alpha_{bf}\upsilon_{bf}}$,

$\mathrm{Pr} = \dfrac{\upsilon_{bf}}{\alpha_{bf}}$ and $Ha = B_0L\sqrt{\dfrac{\sigma_{bf}}{\mu_{bf}}}$.

The dimensionless thermal scenarios are stated as:

For $\tau = 0$,

$$U = 0, V = 0, \theta = 0, P = 0 \quad (19a)$$

For $\tau > 0$,

At the left hot wall:

$$U = 0, V = 0, \theta = 1 \quad (19b)$$

At the top and bottom insulated walls:

$$U = 0, V = 0, \frac{\partial \theta}{\partial Y} = 0 \quad (19c)$$

At the right cold wall: $U = 0, V = 0, \theta = 0$ (19d)

3. Average Nusselt Number (Nu_{ave})

The HT rate is determined by Nu_{ave} at the left heated wall (T_h) that is defined by

$$Nu_{ave} = \int_0^1 Nu_L dY, \; Nu_L = -\frac{\kappa_{hnf}}{\kappa_{bf}} \left(\frac{\partial \theta}{\partial X} \right)_{X=0}.$$

4. Solution systems

4.1. Numerical scheme

The governing equations (15)-(18) along with the thermal sceneries (19a) -(19d) are solved with the finite element method based Galerkin weighted residual strategy. The particulars of this method can be found in the former reports (Rahman et al. 2011, Zienkiewicz and Taylor 1991).

4.2. Grid information

To select the appropriate grid size, a grid assessment is carried out for $\phi_{hnp} = 0.01, Ha = 10,$ $Ra = 10^4, \gamma = \frac{\pi}{6}, \lambda = 0.25, d_p = 130nm, \tau = 0.6, \Pr = 6.8377.$ In the current study, distinct non-uniform grids with the total number of elements (1308, 2124, 3258, 14796 and 55728) are scrutinized. The numerical mode is performed for Nu_{ave} , for the aforementioned elements to clarify the grid quality as displayed in Table 2. It is observed that the outputs of the Nu_{ave} for 14796 elements exhibit a very little change with the results obtained for the elements 55728. Therefore, here is chosen 14796 triangular elements to solve the HT of the H-NF model with accurate results.

Table 2: Grid information for $Al_2O_3 - Cu$ / *water* H-NF, when $Ha = 10, Ra = 10^4, \phi_{hnp} = 0.01, \lambda = 0.25,$ $\gamma = \frac{\pi}{6}, d_p = 130nm, \tau = 0.6.$

Objects	Norma1	Fine	Finer	Extra Fine	Extremely Fine
Number of elements	1308	2124	3258	14796	55728
Number of Nodes	701	1121	1702	7553	28165
Nu_{ave}	1.576	1.589	1.596	1.608	1.610
Degrees of Freedom	2804	4484	6808	30212	112660

4.3. Code validation

To authenticate the accuracy, the existing numerical code is compared with the prior investigation of (Ho et al. 2010). Three dissimilar NPs VF with $Al_2O_3 - H_2O$ NF are considered in this validation as well. The tested cavity is a four-sided outline with thermal gradients between lateral walls with thermally insulated bottom and top walls. Table 3 displays the comparison of the current outputs of the Nu_{ave} , and the previous results of (Ho et al. 2010) for dissimilar values

Table3: Comparison of the current outputs Nu_{ave} with Ho et al. (2010) for dissimilar values of NPs VF (ϕ).

ϕ	Ho et al. (2010) (Nu_{ave})	Present study (Nu_{ave})	Error (%)
0.01	31.8633	32.2541	1.22
0.02	31.5112	31.1234	1.23
0.03	28.1206	28.8452	2.57

Table 4: Comparison of the current outputs Nu_{ave} with Ghasemi et al. (2011) for different values of *Ha*

and ϕ.

	ϕ = 0.02			ϕ = 0.04		
Ha	Ghasemi et al. (2011)	Present study	Error (%)	Ghasemi et al. (2011)	Present study	Error (%)
0	4.820	4.831	0.23	4.896	4.912	0.33
15	4.179	4.182	0.07	4.211	4.217	0.14
30	3.138	3.142	0.13	3.124	3.127	0.10
45	2.342	2.382	1.70	2.317	2.320	0.13
60	1.831	1.861	1.63	1.815	1.826	0.61

of NPs VF. Secondly, our applied solution methodology is also validated in the case of Al_2O_3-H_2O nanofluid with $\phi = 0.02$ and $\phi = 0.04$ with those Ghasemi et al. (2011). These comparisons are displayed in Table 4 in terms of Nu_{ave} for various values of *Ha* .These validations encouraging the assurance in the numerical precision of the current study.

5. Results and discussion

The obtained results are discussed to examine the impacts of IPMF intensity of the square cavity filled with $Al_2O_3 - Cu / water$ H-NF having uniform thermal BCs at the T_h . The ranges of the

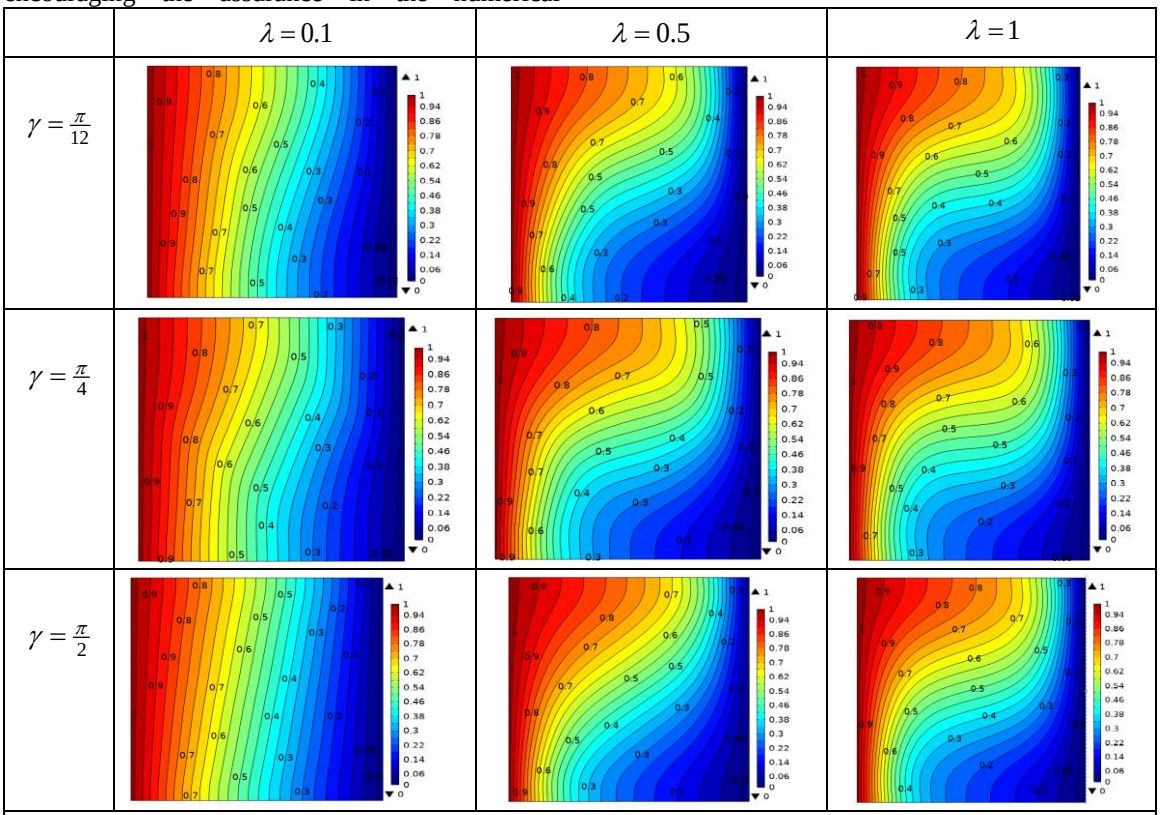

Fig. 2: Isotherms pattern for dissimilar values of γ and λ when $\phi_{hnp} = 0.01, Ha = 10, Ra = 10^4$, $d_p = 130nm, \tau = 0.6$.

dimensionless temperature of the fluid in the isothermal contours are obtained from 0 to 1. Estimations are prepared for different values of the pertinent parameters γ of the slanted PMF, period (λ) of the IPMF, Ha, Ra , and hybrid NPs VF

$0 \le \phi_{hnp} \le 0.025$. The outcomes are enunciated with isotherms and Nu_{ave} at the T_h for dissimilar model parameters. In the whole study the hybrid NPs VF is fixed with equal VF of the NPs. The core focus of the outcomes is to find a precise idea of the HT for H-NF filled square cavity for industrial uses. The joint effects of the γ and λ of the IPMF for $\gamma = \frac{\pi}{12}, \frac{\pi}{4}, \frac{\pi}{2}; \lambda = 0.1, 0.5, 1$ on the isotherms are presented in Fig.2. It is obvious from this figure that isotherms are closer near the T_h of the cavity. Therefore, the thermal gradient at the cavity near the T_h is larger than cold wall, that deliberates higher HT at the T_h of the cavity. The γ shows higher effect on the isotherm's patterns at $\gamma = \pi / 4$. There is an expansion of thickness of the thermal scenery layer with the rise of the γ. From this figure we also see that as the λ of the slanted PMF increases, the intensity of the isotherm increases, this means that the λ of the inclined PMF play a vital role in HT analysis.

The joint impacts of Ha and Ra for $Ha = 15, 40, 80;\ Ra = 10^4, 10^5, 10^6$ on the isotherms are viewed in Fig.3. The isotherms show a critical role in HT using H-NF since they express us which modes of HT are effective and how strong is the convection. This figure shows that isotherms are closer near T_h of the cavity. Therefore, the thermal

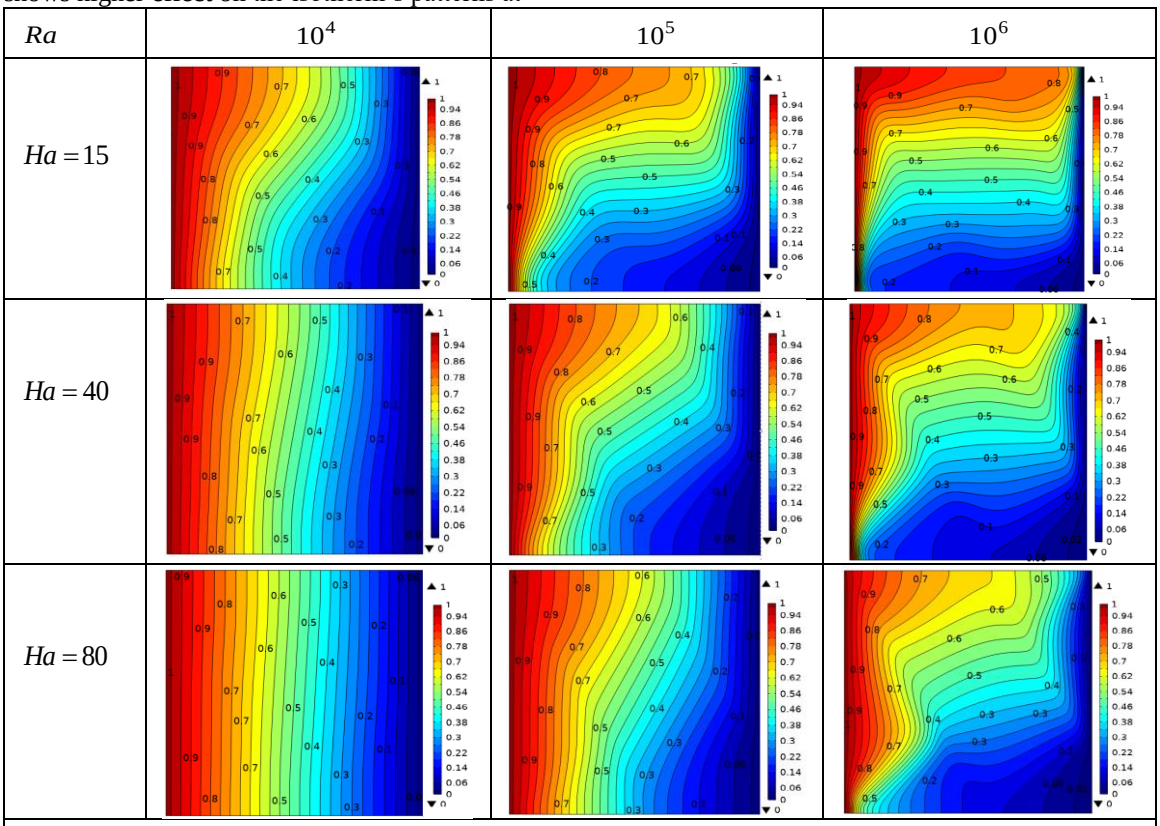

Fig. 3: Isotherms pattern for different values of Ra & Ha when $\phi_{hnp} = 0.01, \lambda = 0.25, \gamma = \frac{\pi}{6}, d_p = 130nm, \tau = 0.6.$

gradient at the cavity near the T_h is larger than cold wall, that reflects more HT at the T_h of the cavity. As the Ha rises, the isothermal lines are squished closer to the T_h, which is a clear sign that convection is the dominant mechanism of heat spread. Also, for any values of Ra, the cohesiveness of the isotherm drops as the Ha rises, indicating a switch from convection to conduction as the method of heat transport. For nanofluid flow with low value of Ra, the isotherms are almost vertical since heat is conveyed by conduction between the hot and cold walls. Convection inside the cavity also strengthens as a result of growing values of the Ra, or for bigger temperature gradients; the isotherms become increasingly skewed towards the cold side walls, and the buoyancy upward movement occupies nearly the whole cavity. Thus, for larger values of Ra (Ra = 10^6), the warm fluid from the cavity's left flows quite quickly, transferring more heat to the right cold wall.

The profiles of Nu_{ave} versus λ for dissimilar values of γ along the T_h are shown in Fig.4a, when $\phi_{hnp} = 0.01, Ra = 10^4, Ha = 10, d_p = 130nm, \tau = 0.6$. From this figure we see that the Nu_{ave} increases with the raise of λ and strongly depends on the γ. Thus, both the γ and λ play a momentous role on the HT analysis. Observe from the Fig.4a that the extreme thermal performance is found at an inclination angle $\gamma = \frac{\pi}{4}$ and $\lambda = 1$.

The distribution of the Nu_{ave} versus the Ra for unlike values of the Ha along the T_h are plotted in Fig. 4b, when $\phi_{hnp} = 0.01, \gamma = \frac{\pi}{6}, \lambda = 0.25, d_p = 130nm, \tau = 0.6$. From this figure, it is observed that the Nu_{ave} upsurges with the increment of the Ra and diminutions with the increment of the Ha. A high Ra agrees to a strong buoyancy force that specifies more thermal energy to the system. Therefore, the HT rate from the T_h to the cavity rises. Thus, both the Ha and the Ra play a significant role on the HT analysis.

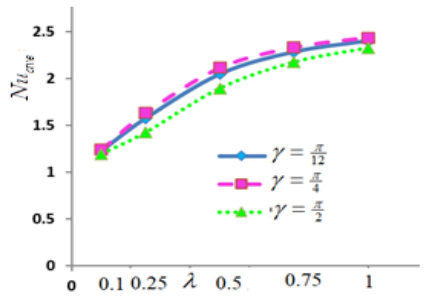

Fig. 4a. Distribution of Nu_{ave} versus λ for different values of inclination angle γ.

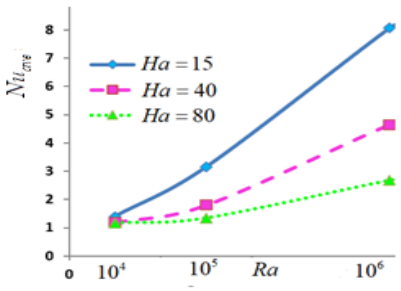

Fig. 4b. Distribution of Nu_{ave} versus Ra for different values of *Ha.*

Table 5. Nu_{ave} along T_h for pure fluid(water), NF and H-NF for dissimilar values of ϕ_{hnp} and Ra, when $Ha = 10, \gamma = \frac{\pi}{6}, \lambda = 0.25, \tau = 0.6.$

Items	ϕ_{hnp}	Nu_{ave}		
		$Ra = 10^4$	$Ra = 10^5$	$Ra = 10^6$
Pure water	0	1.4063	3.3852	7.9589
Nanofluid	0.005	1.4958	3.5935	8.5597
	0.01	1.5867	3.7989	9.0734
	0.02	1.7768	4.2232	10.138
	0.025	1.8756	4.4417	10.688
Hybrid nanofluid	0.005	1.5050	3.6096	8.5850
	0.01	1.6078	3.8468	9.1685
	0.02	1.8237	4.3416	10.388
	0.025	1.9371	4.5989	11.024

Table 6. Nu_{ave} (with/without Brownian effect) along left heated wall for dissimilar values of Ra and ϕ_{hnp}, when $Ha = 10, \gamma = \frac{\pi}{6}, \lambda = 0.25,\ d_p = 130nm, \tau = 0.6.$

Ra	ϕ_{hnp}	Nu_{ave}			
		With Brownian effect	Increase (%)	Without Brownian effect	Increase (%)
10^4	0.005	1.5050	7.02	1.4468	2.88
	0.01	1.6078	14.33	1.4891	5.89
	0.02	1.8237	29.68	1.5751	12.00
	0.025	1.9371	37.74	1.6193	15.14
10^5	0.005	3.6096	6.63	3.4766	2.70
	0.01	3.8468	13.64	3.5756	5.62
	0.02	4.3416	28.25	3.7778	11.60
	0.025	4.5989	35.85	3.8815	14.66
10^6	0.005	8.5850	7.87	8.2558	3.73
	0.01	9.1685	15.20	8.2999	4.28
	0.02	10.388	30.52	8.9883	12.93
	0.025	11.024	38.51	9.2405	16.10

Table 5 illustrates the variation of Nu_{ave} along T_h for BF (pure water), NFs and H-NF for dissimilar values of NPs VF and Ra, when $Ha = 10,\ \lambda = 0.25, \gamma = \frac{\pi}{6},\ d_p = 130nm, \tau = 0.6.$ This table shows that as the NPs VF and the Ra rises, the Nu_{ave} is also rises for all types of smart fluids. Also, the better HT rate is obtained for H-NF.

Table 6 demonstrates the Nu_{ave} (with or without Brownian effect) along T_h for dissimilar values of Ra and ϕ_{hnp}, when $Ha = 10, \gamma = \frac{\pi}{6}, \lambda = 0.25,\ d_p = 130nm, \tau = 0.6.$ All the results so found are considering the BM effect on the $Al_2O_3 - Cu / water$ H-NF conductivity, κ_{hnf}, as well-defined in Eq. (13b). It is evident that the BM recognizes a remarkable character in augmentation of the temperature delivery rate. The input of BM is expounded the NPs movement inside the neighborhood which is enhancement the fluidic temperature and micro convection features. Thus, a

comparison study is achieved for the increment of the Nu_{ave} and found from the tabular results that the effect of ϕ_{hnp} on the Nu_{ave} more important for both cases with or without BM. For example, when BM is taken into deliberation, the Nu_{ave} increases 38.51% at $Ra = 10^6$ with $\phi_{hnp} = 0.025$ whereas the corresponding Nu_{ave} increases is 16.10% if the BM of the hybrid NPs is not taken into account. Therefore, we may conclude that the BM of the hybrid NPs plays a vital role on the HT analysis.

6. Conclusions

In the present work, the influences of IPMF on unsteady free convection HT of Al_2O_3-Cu/water H-NF inside a square cavity is studied numerically. The effects of the numerous dimensionless constraints (Ha , λ , γ , Ra, ϕ_{hnp} , and Nu_{ave}) are shown in graphically as well as tabular form. From the current numerical computations, the subsequent inferences are specified as below:

(i) The overall HT rate is reduced with the rising values of the Ha .

(ii) The HT rate is increased when the values of λ , ϕ_{hnp} and Ra rises.

(iii) The highest rate of HT is achieved at $\gamma = \pi / 4$ when $\lambda = 1$.

(iv) When BM of the NPs is taken into discretion of the TC model, the HT rate is increased 38.51% at $Ra = 10^6$ with $\phi_{hnp} = 0.025$ whereas the corresponding increase is16.10% for the case of without BM.

(v) The maximum HT rate is gotten for Al_2O_3-Cu/water hybrid nanofluid.

Nomenclature

Symbols	Descriptions
B_0	Magnetic field strength [$Nm^{-1}A^{-1}$]
c_p	Specific heat [$Jkg^{-1}K^{-1}$]
D_T	Thermal diffusion coefficient [m^2s^{-1}]
D_T^l	Numeric value of D_T
d_p	Diameter of hybrid nanoparticles [nm]
g	Gravitational acceleration [ms^{-2}]
L	Cavity length[m]
Ha	Hartmann number
κ	Thermal conductivity [$Wm^{-1}K^{-1}$]
k_B	Boltzmann constant [JK^{-1}]
Nu	Nusselt number
p	Fluid pressure [Pa]
Pr	Prandtl number
Ra	Rayleigh number
T	FIuid Temperature [K]
t	Dimensional time[s]
c	Cu
c_1	Cold
h	Hot
hnf	Hybrid nanofluid
hnp	Hybrid nanoparticles

Greek symbols

γ	Magnetic field inclination angle rad]
λ	Period
ρ	Density [kgm^{-3}]
τ	Dimensionless time
ϕ	Volume fraction
$\phi_{Al_2O_3}$	Volume fraction of Al_2O_3
ϕ_{Cu}	Volume fraction of Cu
μ	Dynamic viscosity [Nsm^{-2}]
υ	Kinematic viscosity [m^2s^{-1}]
σ	Electric conductivity [s/m]
θ	Dimensionless temperature

Nomenclature

Symbols	**Descriptions**
u, v	Ve1ocity components in x, y directions [ms^{-1}]
U, V	Dimensionless ve1ocity components
x, y	Cartesian coordinates *[m]*
X, Y	Dimensionless coordinates
Subscripts	
a	Al_2O_3
ave	Average
bf	Base fluid
np	Nanoparticles
c	Cu
β	Thermal expansion coefficient [*1/K*]
α	Thermal diffusivity [$m^2 s^{-1}$]
Abbreviations	
BF	Base fluid
HT	Heat transfer
$H-NF$	Hybrid nanofluid
IPMF	Inclined periodic magnetic field
NF	Nanofluid
NP_s	Nanoparticles

Acknowledgements

The authors are grateful to the anonymous reviewers for their constructive comments and suggestions for the further improvement of the paper. Md. Nurul Huda is also grateful to The Ministry of Science and Technology of Bangladesh for providing a doctoral fellowship of this research work.

References

Alam MS, Rahman MM, Parvin S and Vajravelu K. 2016. Finite element simulation for heat line visualization of natural convective flow and heat transfer inside a prismatic enclosure. Int. J. Heat and Technology, 34(3): 391-400.

Belhaj S and Ben-Beya B. 2022. Thermal performance analysis of hybrid nanofluid natural convection in a square cavity containing an elliptical obstacle under variable magnetic field. Int. J. Numer. Meth. Heat&Fluid Flow, 32(6): 1825-1860.

Choi SUS. 1995. Enhancing thermal conductivity of fluids with nanoparticles. In: Signier DA, Wang HP (eds.) Development and applications of non-Newtonian flows. ASME FED, 231(MD66): 99–105.

Devi SU and Devi SA. 2017. Heat transfer enhancement of $Cu-Al_2O_3$ / *water* hybrid nanofluid flow over a stretching sheet. J. Nigerian Mathematical Society, 36(2): 419-433.

Esfe MH, Saedodin S, Yan WM, Afrand M and Sina N. 2016. Study on thermal conductivity of water-based nanofluids with hybrid suspensions of $CNTs / Al_2O_3$ nanoparticles. J. Thermal Analysis and Calorimetry, 124(1): 455-460.

Ghasemi B, Aminossadati SM, and Raisi A. 2011. Magnetic field effect on natural convection in a nanofluid-filled square enclosure, Int. J. Thermal Sciences, 50: 1748-1756.

Ho CJ, Liu WK, Chang YS and Lin CC. 2010. Natural convection heat transfer of alumina-water nanofluid in vertical square enclosure: an experimental study. Int. J. Thermal Sciences,49: 1345-1353.

Izadi M Sheremet MA and Mehryan SAM. 2020. Natural convection of a hybrid nanofluid affected by an inclined periodic magnetic field within a porous medium. Chinese J. Physics, 65:447-458.

Jana S, Salehi-Khojin A and Zhong WH. 2007. Enhancement of fluid thermal conductivity by the addition of single and hybrid nano-additives. Thermochimica Acta, 462(1-2): 45-55.

Maxwell JC. 1873. Electricity and magnetism. Clarendon Press, Oxford, UK.

Nasrin R, Hossain S, Zahan I, Ahmed KFU and Fayaz H. 2020. Performance analysis of hybrid/single nanofluids on augmentation

of heat transport in lid driven undulated cavity. Heat transfer, 49(8): 4204-4225.

Oztop HF and Abu-Nada E. 2008. Numerical study of natural convection in partially heated rectangular enclosures filled with nanofluids, Int. J. Heat and Fluid Flow, 29: 1326-1336.

Rahman MM, Saghir Z and Pop I. 2022. Free convective heat transfer efficiency in $Al_2O_3 - Cu / water$ hybrid nanofluid inside a rectotrapezoidal enclosure. Int. J. Numer. Meth. Heat & Fluid Flow, 32(1): 196-218.

Rahman MM, Parvin S, Saidur R and Rahim NA. 2011. Magnetohydrodynamic mixed convection in a horizontal channel with an open cavity. Int. Commun. Heat and Mass Transfer, 38: 184–193.

Saghir MZ and Rahman MM. 2020. Forced convection of Al_2O_3, Fe_3O_4, $ND - Fe_3O_4$ and $(MWCNT - Fe_3O_4)$ mixtures in rectangular channels: Experimental and numerical results, Int. J. Energy Research,

Suresh S, Venkitaraj KP, Selvakumar P and Chandrasekar M. 2011. Synthesis of $Al_2O_3 - Cu / Water$ hybrid nanofluids using two step method and its thermo physical properties, Colloids and Surfaces. A Physicochemical and Engineering Aspects, 388(1-3): 41- 48.

Selvakumar P and Suresh S. 2012. Use of $Al_2O_3 - Cu / water$ hybrid nanofluid in an electronic heat sink. IEEE transactions on components. Ieee Transactions on Components, Packaging and Manufacturing Technology, 2(10): 1600-1607.

Tayebi T and Oztop HF. 2020. Entropy production during natural convection of hybrid nanofluid in an annular passage between horizontal confocal elliptic cylinders. Int. J. Mechanical Science, 171: 105378.

Zienkiewicz OC and Taylor RL. 1991. The finite element method, 4th Edition, McGraw-Hill.